THE JOURNAL OF PHYSICAL CHEMISTRY Letters

pubs.acs.org/JPCL Letter

Metallic Glacial Glass Formation by a First-Order Liquid−Liquid Transition

J. Shen, Z. Lu, J. Q. Wang, S. Lan, F. Zhang, A. Hirata, M. W. Chen, X. L. Wang, P. Wen, Y. H. Sun,* H. Y. Bai,* and W. H. Wang*

Cite This: J. Phys. Chem. Lett. 2020, 11, 6718−6723 Read Online

ACCESS | Metrics & More | Article Recommendations | Supporting Information

ABSTRACT: The glacial phase, with an apparently glassy structure, can be formed by a first-order transition in some molecular-glass-forming supercooled liquids. Here we report the formation of metallic glacial glass (MGG) from the precursor of a rare-earth-element-based metallic glass via the first-order phase transition in its supercooled liquid. The excellent glass-forming ability of the precursor ensures the MGG to be successfully fabricated into bulk samples (with a minimal critical diameter exceeding 3 mm). Distinct enthalpy, structure, and property changes are detected between MGG and metallic glass, and the reversed "melting-like" transition from the glacial phase to the supercooled liquid is observed in fast differential scanning calorimetry. The kinetics of MGG formation is reflected by a continuous heating transformation diagram, with the phase transition pathways measured at different heating rates taken into account. The finding supports the scenario of liquid−liquid transition in metallic-glass-forming liquids.

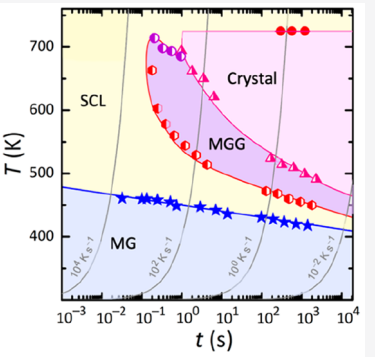

Liquid−liquid transition (LLT) is a first-order phase transition from one liquid to another liquid without the compositional change. LLTs have been reported in many glassy systems like amorphous ice,[1] amorphous silicon,[2] oxide glass,[3] molecular glass,[4,5] and metallic glass (MG) systems.[6−15] To date, the presence of LLT in the metallic liquids at temperatures above the melting temperature (T_m), including the manifestations of abrupt changes of liquid viscosity, the peak position of the diffraction peaks, and the Knight shift in nuclear magnetic resonance, have been reported in many MG systems.[6−11] Meanwhile, signs of LLT in the MG-forming supercooled liquid (SCL),[12−15] including a first-order exothermic transition at temperatures below T_m and above the glass transition temperature (T_g), have been reported. In these cases of the so-called reentrant glass transition, the MG first enters into its SCL via glass transition upon heating; then the SCL transforms to another amorphous phase through LLT; if quenched, new glass of higher T_g is supposed to be made as it has an apparently glassy structure. However, because the formation of this new glass involves a first-order exothermic transition, its nature is unclear owing to the formation mechanism and the threat of undetected nanocrystallization.

Regarding triphenyl phosphite (TPP), a molecular liquid, its LLT in the SCL has attracted great attention.[4,16−25] Since Kivelson et al. first discovered a so-called "glacial phase" in TPP,[16,17] the nature of the glacial phase has been a matter of debate for 20 years. A glacial phase is made when TPP is quenched into a deep SCL and annealed at 210−223 K for several hours. The glacial phase exhibits only broad amorphous halos and no sharp Bragg peaks in X-ray diffraction, reflecting an amorphous nature with an increment of T_g by 20 K, and an energy reduction of 20 J g^{-1} (29% of its heat of fusion, ΔH_F) in comparison with its original glass.[4] The most accepted scenario is that the glacial phase is a new amorphous phase, corresponding to a secondary liquid of TPP. Tanaka et al. revealed a spinodal-decomposition type LLT on annealing under a phase-contrast microscopy[21] and directly accessed the reversibility of LLT without the intervening crystallization at high heating rates in a flash differential scanning calorimetry (FDSC) setup.[25] Furthermore, to describe the structural origin of LLT, a two-order parameter model, with a new parameter, S, added to the conventional order parameter, density, is developed.[4,21] In this model, S is the fraction of locally favored structure in a sea of disordered liquid, and the structural origin of LLT in TTP is a phase transformation from a low-S gas-like liquid to a high-S liquid-like liquid.

In a recent molecular-dynamics simulation, An et al.[26] reported the formation of a G-phase through slow cooling or isothermal annealing in the deeply undercooled metallic Ag liquid by a first-order configurational freezing transition. According to their research, the G-phase is a metastable, heterogeneous, configurationally ordered, and elastically rigid

Received: June 9, 2020
Accepted: July 10, 2020
Published: July 10, 2020

https://dx.doi.org/10.1021/acs.jpclett.0c01789
J. Phys. Chem. Lett. 2020, 11, 6718−6723

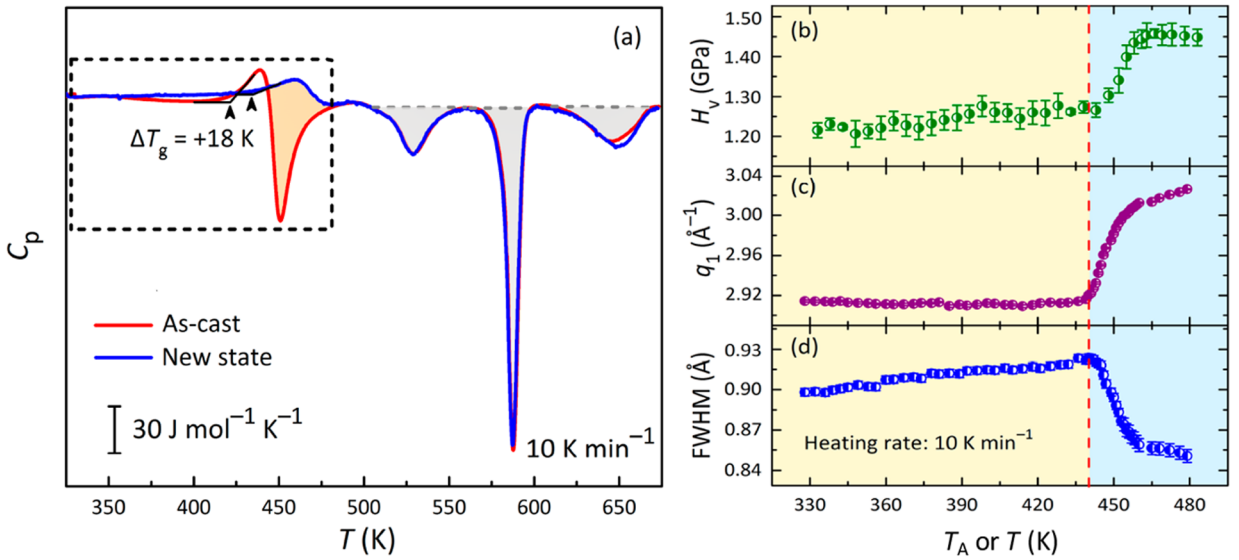

Figure 1. Signs of the first-order LLT in the SCL state of $La_{32.5}Ce_{32.5}Co_{25}Al_{10}$ MG. (a) On heating, the as-cast MG (red curve) exhibits a large exothermic peak (represented by the orange shaded area) immediately after passing its T_g. After quenching the new state (blue curve) from 480 to 330 K and then reheating it, a glass transition is seen, and T_g is enhanced by 18 K. The exothermic peaks presented on further heating (represented by the gray shaded area) are similar between the as-cast and the new state. The dotted box indicates the investigated temperature range in panels b–d. (b) The Vicker hardness (H_V) of one as-cast MG; (c) the peak-position of the first peak in structural factor, q_1; and (d) the FWHM of the first peak in the pair correlation function, show sharp transition during the first post-T_g exotherm of Figure 1a. The hardness is measured at room temperature on one MG whenever it is heated to and cooled from the set annealing temperature T_A. The q_1 and FWHM are measured by synchrotron X-ray scattering during the continuous heating.

glass but has a first-order melting transition toward the high-temperature liquid phase like the crystal. Such a G-phase may well resemble a metallic glacial glass (MGG), similar to that reported in TPP. In the following simulation work, they reported that the G-glass can also be formed in a Cu–Ag binary liquid,[27] suggesting the possibility of forming MGG in a multicomponent alloy. Also recently, Du et al.[14] obtained an ultrastable $Pd_{42.5}Ni_{42.5}P_{15}$ MG by heating its original MG and subsequently cooling its SCL after the LLT. Because of a 50 K increase in T_g and a 1.1 kJ mol^{-1} decrease in the stored energy, this ultrastable MG may be a real example of MGG.

In this Letter, we report the existence of an MGG in $La_{32.5}Ce_{32.5}Co_{25}Al_{10}$ (atom %) composition. Using state-of-the-art technologies, we scrutinize the glassy structure of the MGG made via a first-order LLT in the SCL on heating. The metallic liquid, though atomic in nature, shows very similar LLT to that of the molecular liquid, TTP, being driven by an increased fraction of locally ordered structures as supported by the X-ray diffraction results. Using a fast differential scanning calorimetry (FDSC), we reveal the reversed melting-like transition from MGG to SCL at high heating rates, demonstrating the reversibility of the LLT.

The $La_{32.5}Ce_{32.5}Co_{25}Al_{10}$ (atom %) MG composition was selected for the experiments. The master alloy was prepared by arc-melting the high-purity (>99.5%) elements under a Ti-gettered argon atmosphere. Sheets (1 mm thick), rods (3 mm in diameter), and ribbons (~35 μm thick) were fabricated by either suction casting or melt spinning. Thermal analyses were done on a differential scanning calorimetry instrument (DSC, DSC8000, PerkinElmer) and an FDSC (Flash DSC2+, Mettler Toledo). *In situ* synchrotron X-ray diffraction (SXRD) was measured at station 11-ID-C of the Advanced Photon Source, Argonne National Laboratory, using a 105.721 ± 0.006 keV X-ray beam with a spot size of 0.5 × 0.5 mm^2, while the specimens were heated at 10 K min^{-1} in a furnace (TS1500, Linkam). The transmission electron microscopy (TEM) imaging and diffraction, including the high-resolution TEM (HRTEM) and high angle annular dark-field scanning TEM (HAADF-STEM) measurements, were made on a cold-field emission TEM instrument (JEM-2100F TEM/STEM, JEOL) with double spherical aberration (Cs) correctors at an operation voltage of 200 kV. The selected area electron diffraction (SAED) and the energy dispersive spectroscopy (EDS) mappings were performed in TEM mode and STEM mode, respectively. Nanobeam electron diffraction (NBED) was conducted by utilizing an electron beam with a full width at half-maximum (FWHM) diameter of 3–5 nm. The Vicker hardness (H_v) was measured on a HENGYi MH-51 indenter with an applied load of 500 g. One as-cast MG sheet was repeatedly indented by heating up to temperatures of 353–576 K and then quenching to room temperature.

The calorimetric signal of a potential LLT is found on heating in an as-cast $La_{32.5}Ce_{32.5}Co_{25}Al_{10}$ MG (Figure 1a), as well as in some other rare-earth (RE), transition metal (TM), and aluminum MG (RE-TM-Al) compositions (Figure S1). In calorimetry, the potential LLT is represented by the first post-T_g exothermic peak of this MG. Normally, the post-T_g exothermic peaks of MGs are overlapped, whereas in Figure 1a, those post-T_g exothermic peaks are well-separated. Furthermore, the released heat of the exothermic peaks (represented by the red peak area) is often dominated by one major peak, whereas in this case, the released heat of this MG is similarly distributed by the exothermic peaks. For example, the heat of the first post-T_g peak is 12.3 J g^{-1}, 34.7% of the total heat released by the following three exothermic peaks (Figure S2). Similar results are witnessed in other MG samples of the same composition cut from a sheet and a rod (Figure S3), suggesting that such a post-T_g anomaly is

https://dx.doi.org/10.1021/acs.jpclett.0c01789
J. Phys. Chem. Lett. 2020, 11, 6718–6723

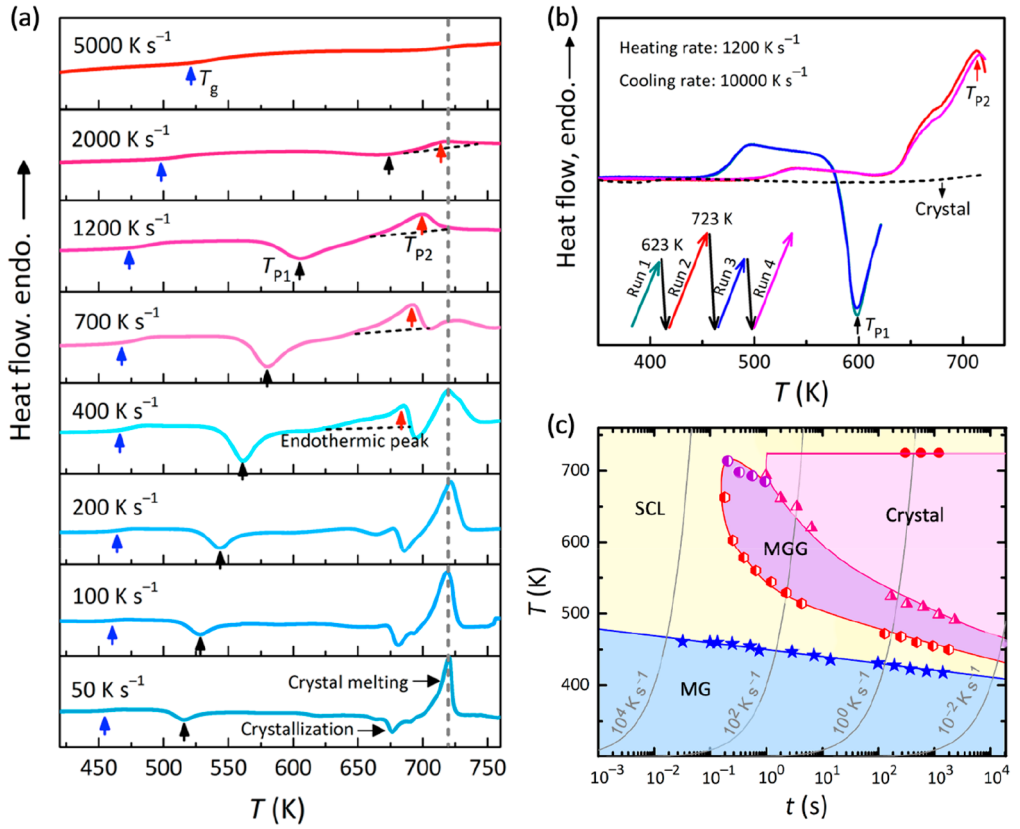

Figure 2. FDSC analyses of LLT at a series of fast heating rates. (a) For the MG, multiple exotherms appear after the LLT at 50−200 K s^{-1}; a new endothermic peak appears before the main melting peak while other exotherms except the LLT disappear at 400−2000 K s^{-1}; no exotherms and endotherms are detected at 5000 K s^{-1}. The T_g, peak temperature of the exothermic and endothermic peaks, T_{p1} and T_{p2}, are marked by blue, black and red arrows. (b) No endothermic peak is detected when heating the crystals so that the endothermic peaks detected on run 2 and run 4 are not the melting of crystals. (c) The continuous heating transformation diagram of the MG. At low heating rate (ϕ), the transitions of MG to SCL, SCL to MGG, and MGG to crystal are intervened; at moderate ϕ, MG to SCL, SCL to MGG, and MGG to SCL are bypassed; at high ϕ, only MG to SCL is exhibited.

independent of sample size. Upon heating the as-cast sample to the end temperature of the first post-T_g peak (480 K) and then cooling it to room temperature, a new state is obtained. In the subsequent heating, the post-T_g peak disappears while the other three exothermic peaks remain unchanged. However, an unexpected "glass transition" of the new state is detected because one would not expect to see glass transition if the new state is a crystalline phase (Figure S2); the results from HRTEM, NBED, and SXRD confirm its amorphicity (Figure 3). Thus, in analogy with TPP, the glass cooled from the new state is termed as the MGG. For comparison, in the following context, we use MG to represent the as-cast glass. Furthermore, the T_g, defined by the onset of an increase in heat capacity (C_p), is enhanced by 18 K (from 420 to 438 K), a magnitude that is similar to that observed for ultrastable glassy thin films.[28,29] Moreover, the MGG has a broader glass transition, suggesting the new state is stronger than the as-cast state. The first-order nature of this exothermic event is also witnessed by its corresponding evolution in property and structure. For the H_V, an abrupt increase occurs at the onset temperature of this post-T_g exotherm, and the final enhancement of H_V is as large as 20% (Figure 1b), consistent with increase of shear modulus of the G-glass as observed in molecular dynamics simulation.[27] In addition, the peak-position shift of the first maximum of $S(q)$, q_1, sharply increases at the onset temperature (Figure 1c). Similarly, the FWHM of the first peak in pair correlation function, $g(r)$, as an indicator of the configurational entropy,[30,31] is suddenly decreased when passing the onset temperature in heating (Figure 1d). In comparison with another MG without such post-T_g exotherm, no significant changes of q and FWHM in heating are detected (Figure S4). Hence, the abrupt change of energy, property, and structure detected above are signs of a first-order transition.

When heating the MGG at high ϕ's (50 to 5000 K s^{-1}) in FDSC, we also observe a melting-like endothermic peak, as predicted in the simulations of Ag (ref 26) and Cu−Ag (ref 27) and revealed in the experiment of TPP (ref 25). As shown in Figure 2a, both T_g and the peak temperature of the first post-T_g exotherm (T_{p1}) get gradually separated from the increasing ϕ. At ϕ = 50−400 K s^{-1}, other exothermic peaks, representing crystallization (Figure S5), are observed. At ϕ = 700−2000 K s^{-1}, the exothermic peak of the potential LLT is directly followed by an endothermic peak, with a peak temperature defined as T_{p2}, instead of other exotherm peaks. At ϕ > 5000 K s^{-1} no exothermic and endothermic peaks are detected anymore. The results imply that the endothermic peak detected at ϕ = 700−2000 K s^{-1} may be the reversible event of the exothermic peak, because the endotherm is undetected when the exotherm doesn't appear at ϕ > 5000 K s^{-1}. Besides, the area of this endothermic peak is comparative with that of the exothermic peak, once again suggesting the

https://dx.doi.org/10.1021/acs.jpclett.0c01789
J. Phys. Chem. Lett. 2020, 11, 6718−6723

reversibility. The LLT and its reverse process do not proceed at the same transition temperature because undercooling is required for the LLT, as crystallization takes place below the melting temperature. To prove the reversibility, the as-cast specimen is heated to 623 K at 1200 K s^{-1} and cooled to 300 K at 10000 K s^{-1} to make the new state *in situ* (Figure 2b). Next, the new state is heated to 723 K at 1200 K s^{-1}, quenched at 10000 K s^{-1}, and reheated at 1200 K s^{-1}(inset in Figure 2b). Note this endotherm is not melting because when a crystallized sample is measured at the same ϕ, its melting cannot be detected up to 723 K. The results show that the third heating trace matches well with the first heating, reflecting that the product quenched from the 723 K is a recovered glassy state of the as-cast sample.

Figure 2c is a continuous heating transformation (CHT) diagram, involving the data measured at different ϕ, which describes all the possible transformation pathways of the MG on heating. Four regions are defined by these temperatures, including the MG, its SCL, the MGG, and the crystal. At low ϕ (ϕ < 400 K s^{-1}), the glass transition (MG to SCL), the LLT (SCL to MGG), and the crystallization (MGG to crystal) are always detected. At high ϕ (ϕ = 5000 K s^{-1}), heating is too fast to allow LLT to take place so that only the glass transition shows up. However, in a narrow range of ϕ (700 < ϕ < 2000 K s^{-1}), the transformation of MGG to crystal is avoided, and hence, the reverse process of LLT (MGG to SCL) occurs.

The MGG, made by quenching down to room temperature after LLT, is checked under various state-of-the-art structural characterization techniques. To exclude the possibility of nanocrystals or quasi-crystals, HRTEM, SAED, NBED, and SXRD were applied to examine both the MGG (Figure 3a–d) and the MG (Figure S6). The typical disordered maze-like atomic structure suggests an amorphous structure of the MGG (Figure 3a). The corresponding SAED pattern further proves the absence of nanocrystals or quasi-crystals (Figure 3b). In the NBED pattern, the diffraction spots at the first diffraction ring, representing the short-range order of the new state, are presented, and the absence of bright diffraction spots confirms that the new state is fully amorphous (Figure 3c). In all the cases, only glass structures or amorphous halos are observed, and neither nanocrystals nor quasi-crystals are detected. Also, no compositional segregations associated with phase separation[31] are detected above a nanometer-length-scale as suggested by EDS (Figure S7). The pair-correlation functions $g(r)$ (Figure 3e) and the total structural factor $S(q)$ (inset in Figure 3e) of both the MGG and the MG verify the absence of long-range translational symmetry. However, signs of medium-range order[30] appear in $g(r)$ and $S(q)$ of the MGG. For example, the intensity of the second halo is enhanced, while an extra peak appears on its shoulder around 4.54 $Å^{-1}$ for the MGG. Furthermore, $g(r)$ of the MGG exhibits well-defined oscillations up to 17 Å, right within the medium atomic-pair range. Moreover, the FWHM of the first nearest-neighbor shell is narrowed by −5.6% from 0.90 to 0.85 Å, indicating a more ordered structure and a decrease in the configurational entropy.[30−32] In contrast, the HRTEM and NBED of nanocrystals have clear periodic atomic-packing structures and high-q signals, respectively (Figure S8), totally different from the observations made on this MGG. Therefore, the MGG is confirmed to be not a nanocrystal but more likely a glass with different short-range order in comparison to the original MG.

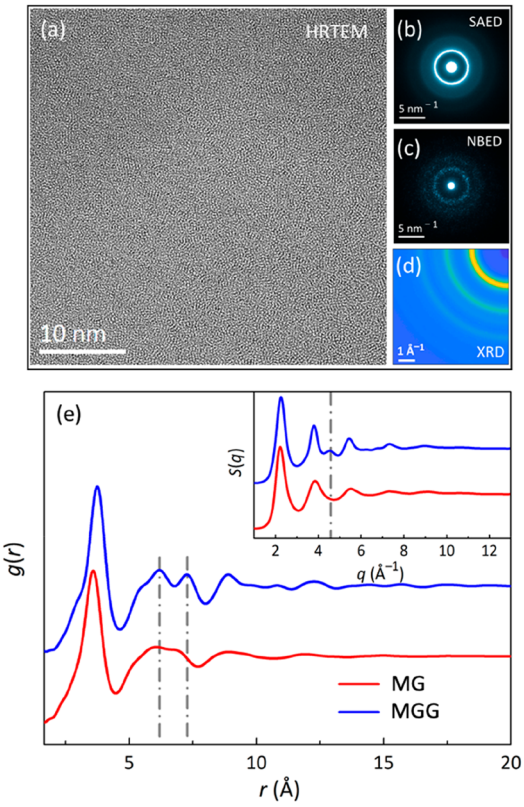

Figure 3. Structural characterization of the MGG. No crystalline phases are detected under the examination of high-resolution transmission electron microscopy (HRTEM) imaging (a), selected area electron diffraction (SAED) (b), nanobeam electron diffraction (NBED) (c), and synchrotron X-ray diffraction (SXRD) (d). The pair correlation function $g(r)$ and the structural factor $S(q)$ (inset) of the MG and the MGG are compared in panel e. The split of the second peak in both $g(r)$ and $S(q)$ of the MGG is marked by dotted lines.

From the traditional viewpoint, density is the single order-parameter used for the description of the liquid state only.[33] Apart from the counterintuitive impression on the coexistence of liquids with two different densities,[25] little density changes between the MGG and the MG are detected. At room temperature, the density of the MGG is 6.83 ± 0.30 g cm^{-3}, similar to that of the MG, 6.80 ± 0.30 g cm^{-3}. On the other hand, synchrotron X-ray scattering reveals that first, the FWHM of the first peak of g(r) is reduced after LLT (Figure 1d), representing a lowering of entropy and an ordering of structure; second, new peaks are detected on the originally broad amorphous halos at r > 5 Å (Figure 3e), implying an unambiguous structural ordering in the range of 5–20 Å. In comparison with the molecular dynamics simulations of G-phase in the Cu–Ag binary alloy, the length scale of the ordered region of MGG is consistent with the correlation length of the G-phase, i.e., from several nanometers in the elemental metals to ∼1 nm at the eutectic composition.[27] Such a discrete feature of diffraction is typical for the icosahedral clusters,[34] i.e., the locally favored structural units of MGs, as a similar discrete partial reduced radial distribution function is reported by molecular dynamics simulation of a $Ni_{80}P_{20}$ MG.[35] Thus, the ordering process of MG during LLT is likely to be another example of the local atomic bond ordering or the fraction increase of the locally favored structures typically observed in TPP.[4,21]

https://dx.doi.org/10.1021/acs.jpclett.0c01789
J. Phys. Chem. Lett. 2020, 11, 6718−6723

The glacial phase of TPP has a T_g of 225 K (ref 21), which is below room temperature, whereas the MGG has a T_g of 438 K, which is above room temperature. The stability of the MGG at the ambient condition makes it a possible candidate to be applied as a new engineering material. Preliminary results show an 18 K increase in T_g (Figure 1a) and a 20% increase in hardness (Figure 1b) of the MGG, which is unusual in comparison to the change of MG induced by conventional annealing. The great reduction in enthalpy of 12.3 J g^{-1} implies that the MGG is at a thermodynamically ultrastable state.[36] Because the thin-film ultrastable glasses are often made in a kinetic manner via slow deposition,[28,29] the first-order LLT of MG may become a useful alternative to make ultrastable bulk MG in a thermodynamic manner. Indeed, the MGG rods, 3 mm in diameter, and sheets, 1 mm in thickness, are successfully made in our experiments (Figure S3), providing a good candidate for further investigations.

In summary, using high-resolution transmission electron microscopy, in situ synchrotron X-ray diffraction, and flash differential scanning calorimetry, we reveal the existence of a metallic glacial glass in a rare-earth-element-based metallic glass composition. The metallic glacial glass exhibits thermodynamic ultrastability and a big increase in hardness by 20% in comparison with its original metallic glass. Different from the original metallic glass, the metallic glacial glass exhibits a first-order melting-like transition upon rapid heating, which is the reverse process of its freezing formation. The existence of metallic glacial glass indicates that two liquids settle in their respective temperature regions, supporting the scenario of liquid−liquid transition in the metallic-glass-forming supercooled liquid. Therefore, the new metallic glacial glass provides a useful example for future research of the liquid−liquid transition in the atomic liquid system.

■ ASSOCIATED CONTENT

Supporting Information

The Supporting Information is available free of charge at https://pubs.acs.org/doi/10.1021/acs.jpclett.0c01789.

Experimental details; Figure S1 showing calorimetry for the MG and the MGG of six different compositions; Figure S2 showing calorimetry curves of the as-cast MG and the crystallized $La_{32.5}Ce_{32.5}Co_{25}Al_{10}$; Figure S3 showing the calorimetry for the MG in three different casting forms; Figure S4 showing the structural evolution of MG on heating under synchrotron X-ray scattering; Figure S5 showing the $S(q)$ changes of MG on heating; Figure S6 displaying the HRTEM, SAED, and NBED of the MG; Figure S7 displaying the EDS mapping of the MGG; Figure S8 displaying the HRTEM and NBED of the sample with nanocrystals (PDF)

■ AUTHOR INFORMATION

Corresponding Authors

Y. H. Sun − *Institute of Physics, Chinese Academy of Sciences, Beijing 100190, China; School of Physical Sciences, University of Chinese Academy of Sciences, Beijing 100049, China; Songshan Lake Materials Laboratory, Dongguan, Guangdong 523808, China;* orcid.org/0000-0003-3987-1711; Email: ysun58@iphy.ac.cn

H. Y. Bai − *Institute of Physics, Chinese Academy of Sciences, Beijing 100190, China; Songshan Lake Materials Laboratory, Dongguan, Guangdong 523808, China; Center of Materials Science and Optoelectronics Engineering, University of Chinese Academy of Sciences, Beijing 100049, China;* orcid.org/0000-0001-7687-7624; Email: hybai@iphy.ac.cn

W. H. Wang − *Institute of Physics, Chinese Academy of Sciences, Beijing 100190, China; School of Physical Sciences, University of Chinese Academy of Sciences, Beijing 100049, China; Songshan Lake Materials Laboratory, Dongguan, Guangdong 523808, China;* Email: whw@iphy.ac.cn

Authors

J. Shen − *Institute of Physics, Chinese Academy of Sciences, Beijing 100190, China; School of Physical Sciences, University of Chinese Academy of Sciences, Beijing 100049, China*

Z. Lu − *Mathematics for Advanced Materials - Open Innovation Laboratory (MathAM-OIL), AIST, Sendai 980-8577, Japan*

J. Q. Wang − *School of Physical Sciences, University of Chinese Academy of Sciences, Beijing 100049, China; Ningbo Institute of Materials Technology and Engineering, Chinese Academy of Sciences, Ningbo 315201, China*

S. Lan − *Herbert Gleiter Institute of Nanoscience, Nanjing University of Science and Technology, Nanjing 210094, China; Department of Physics and Materials Science, City University of Hong Kong, Hong Kong, China*

F. Zhang − *WPI- Advanced Institute for Materials Research (WPI-AIMR), Tohoku University, Sendai 980-8577, Japan*

A. Hirata − *WPI- Advanced Institute for Materials Research (WPI-AIMR), Tohoku University, Sendai 980-8577, Japan*

M. W. Chen − *Department of Materials Science and Engineering, Johns Hopkins University, Baltimore, Maryland 21218, United States*

X. L. Wang − *Department of Physics and Materials Science and Center for Advanced Structural Materials, City University of Hong Kong, Hong Kong, China; City University of Hong Kong Shenzhen Research Institute, Shenzhen 518057, China*

P. Wen − *Institute of Physics, Chinese Academy of Sciences, Beijing 100190, China; School of Physical Sciences, University of Chinese Academy of Sciences, Beijing 100049, China*

Complete contact information is available at: https://pubs.acs.org/10.1021/acs.jpclett.0c01789

Notes

The authors declare no competing financial interest.

■ ACKNOWLEDGMENTS

We acknowledge Prof. A. L. Greer, Prof. Y. Wu, Prof. J. Perepezko, and Dr. Jiri Orava for stimulating discussions. Prof. Yanhui Liu, Prof. Baoan Sun, Dr. Lijian Song, and Ms. Yaru Cao are appreciated for experimental assistance. This research was supported by the Strategic Priority Research Program of the Chinese Academy of Sciences (XDB30000000), National Key Research and Development Plan (2018YFA0703603), National Natural Science Foundation of China (11790291, 61999102, 61888102, and 51971238), and Natural Science Foundation of Guangdong Province (2019B030302010).

■ REFERENCES

(1) Mishima, O.; Calvert, L. D.; Whalley, E. 'Melting ice I' at 77 K and 10 kbar: a new method of making amorphous solids. *Nature* **1984**, *310*, 393−395.

(2) Vasisht, V. V.; Saw, S.; Sastry, S. Liquid-liquid critical point in supercooled silicon. *Nat. Phys.* **2011**, *7*, 549−553.

(3) Aasland, S.; McMillan, P. F. Density-driven liquid-liquid phase separation in the system Al_2O_3-Y_2O_3. *Nature* **1994**, *369*, 633−636.

https://dx.doi.org/10.1021/acs.jpclett.0c01789
J. Phys. Chem. Lett. 2020, 11, 6718−6723

(4) Tanaka, H.; Kurita, R.; Mataki, H. Liquid-liquid transition in the molecular liquid triphenyl phosphite. *Phys. Rev. Lett.* **2004**, *92*, 025701.
(5) Zhu, M.; Wang, J. Q.; Perepezko, J. H.; Yu, L. Possible existence of two amorphous phases of d-mannitol related by a first-order transition. *J. Chem. Phys.* **2015**, *142*, 244504.
(6) Li, J. J. Z.; Rhim, W. K.; Kim, C. P.; Samwer, K.; Johnson, W. L. Evidence for a liquid-liquid phase transition in metallic fluids observed by electrostatic levitation. *Acta Mater.* **2011**, *59*, 2166−2171.
(7) Jonas, I.; Yang, F.; Meyer, A. Long-range mass transport during structure transitions in metallic glass-forming melts. *Phys. Rev. Lett.* **2019**, *123*, 055502.
(8) Wei, S.; Yang, F.; Bednarcik, J.; Kaban, I.; Shuleshova, O.; Meyer, A.; Busch, R. Liquid-liquid transition in a strong bulk metallic glass-forming liquid. *Nat. Commun.* **2013**, *4*, 2083.
(9) Zhou, C.; Hu, L. N.; Sun, Q. J.; Qin, J. Y.; Bian, X. F.; Yue, Y. Z. Indication of liquid-liquid phase transition in CuZr-based melts. *Appl. Phys. Lett.* **2013**, *103*, 171904.
(10) Xu, W.; Sandor, M. T.; Yu, Y.; Ke, H. B.; Zhang, H. P.; Li, M. Z.; Wang, W. H.; Liu, L.; Wu, Y. Evidence of liquid-liquid transition in glass-forming $La_{50}Al_{35}Ni_{15}$ melt above liquidus temperature. *Nat. Commun.* **2015**, *6*, 7696.
(11) Küchemann, S.; Samwer, K. Ultrafast heating of metallic glasses reveals disordering of the amorphous structure. *Acta Mater.* **2016**, *104*, 119−124.
(12) Stolpe, M.; Jonas, I.; Wei, S.; Evenson, Z.; Hembree, W.; Yang, F.; Meyer, A.; Busch, R. Structure changes during a liquid-liquid transition in the deeply undercooled $Zr_{58.5}Cu_{15.6}Ni_{12.8}Al_{10.3}Nb_{2.8}$ bulk metallic glass forming melt. *Phys. Rev. B: Condens. Matter Mater. Phys.* **2016**, *93*, 014201.
(13) Lan, S.; Ren, Y.; Wei, X. Y.; Wang, B.; Gilbert, E. P.; Shibayama, T.; Watanabe, S.; Ohnuma, M.; Wang, X. L. Hidden amorphous phase and reentrant supercooled liquid in Pd-Ni-P metallic glasses. *Nat. Commun.* **2017**, *8*, 14679.
(14) Du, Q.; Liu, X. J.; Fan, H. Y.; Zeng, Q. S.; Wu, Y.; Wang, H.; Chatterjee, D.; Ren, Y.; Ke, Y. B.; Voyles, P. M.; Lu, Z. P.; Ma, E. Reentrant glass transition leading to ultrastable metallic glass. *Mater. Today* **2020**, *34*, 66−77.
(15) Lou, H. B.; Zeng, Z. D.; Zhang, F.; Chen, S. Y.; Luo, P.; Chen, X. H.; Ren, Y.; Prakapenka, V. B.; Prescher, C.; Zuo, X. B.; Li, T.; Wen, J. G.; Wang, W. H.; Sheng, H. W.; Zeng, Q. S. Two-way tuning of structural order in metallic glasses. *Nat. Commun.* **2020**, *11*, 314.
(16) Cohen, I.; Ha, A.; Zhao, X. L.; Lee, M.; Fischer, T.; Strouse, M. J.; Kivelson, D. A low-temperature amorphous phase in a fragile glass-forming substance. *J. Phys. Chem.* **1996**, *100*, 8518−8526.
(17) Ha, A.; Cohen, I.; Zhao, X.; Lee, M.; Kivelson, D. Supercooled liquids and polyamorphism. *J. Phys. Chem.* **1996**, *100*, 1−4.
(18) Johari, G. P.; Ferrari, C. Calorimetric and dielectric investigations of the phase transformations and glass transition of triphenyl phosphite. *J. Phys. Chem. B* **1997**, *101*, 10191−10197.
(19) Demirjian, B. G.; Dosseh, G.; Chauty, A.; Ferrer, M. L.; Morineau, D.; Lawrence, C.; Takeda, K.; Kivelson, D.; Brown, S. Metastable solid phase at the crystalline-amorphous border: The glacial phase of triphenyl phosphite. *J. Phys. Chem. B* **2001**, *105*, 2107−2116.
(20) Hédoux, A.; Guinet, Y.; Descamps, M.; Hernandez, O.; Derollez, P.; Dianoux, A. J.; Foulon, M.; Lefèbvre, J. A description of the frustration responsible for a polymorphism situation in triphenyl phosphite. *J. Non-Cryst. Solids* **2002**, *307−310*, 637−643.
(21) Kurita, R.; Tanaka, H. Critical-like phenomena associated with liquid-liquid transition in a molecular liquid. *Science* **2004**, *306*, 845−848.
(22) Shimizu, R.; Kobayashi, M.; Tanaka, H. Evidence of liquid-liquid transition in triphenyl phosphite from time-resolved light scattering experiments. *Phys. Rev. Lett.* **2014**, *112*, 125702.
(23) Kobayashi, M.; Shimizu, R.; Tanaka, H. Time-resolved light scattering study on the kinetics of liquid-liquid transition in triphenyl phosphite. *J. Phys. Chem. B* **2015**, *119*, 11768−11782.
(24) Murata, K.; Tanaka, H. Microscopic identification of the order parameter governing liquid-liquid transition in a molecular liquid. *Proc. Natl. Acad. Sci. U. S. A.* **2015**, *112*, 5956−5961.
(25) Kobayashi, M.; Tanaka, H. The reversibility and first-order nature of liquid-liquid transition in a molecular liquid. *Nat. Commun.* **2016**, *7*, 13438.
(26) An, Q.; Johnson, W. L.; Samwer, K.; Corona, S. L.; Goddard, W. A., III First-order phase transition in liquid Ag to the heterogeneous G-phase. *J. Phys. Chem. Lett.* **2020**, *11*, 632−645.
(27) An, Q.; Johnson, W. L.; Samwer, K.; Corona, S. L.; Goddard, W. A., III Formation of two glass phases in binary Cu-Ag liquid. *Acta Mater.* **2020**, *195*, 274−281.
(28) Swallen, S. F.; Kearns, K. L.; Mapes, M. K.; Kim, Y. S.; McMahon, R. J.; Ediger, M. D.; Wu, T.; Yu, L.; Satija, S. Organic glasses with exceptional thermodynamic and kinetic stability. *Science* **2007**, *315*, 353−356.
(29) Yu, H. B.; Luo, Y. S.; Samwer, K. Ultrastable metallic glass. *Adv. Mater.* **2013**, *25*, 5904−5908.
(30) Hufnagel, T. C.; Brennan, S. Short- and medium-range order in $(ZrCuNi)_{(90-x)}Ta_xAl_{10}$ bulk amorphous alloys. *Phys. Rev. B: Condens. Matter Mater. Phys.* **2003**, *67*, 014203.
(31) Hufnagel, T. C.; Ott, R. T.; Almer, J. Structural aspects of elastic deformation of a metallic glass. *Phys. Rev. B: Condens. Matter Mater. Phys.* **2006**, *73*, 064204.
(32) Kim, D. H.; Kim, W. T.; Park, E. S.; Mattern, N.; Eckert, J. Phase separation in metallic glasses. *Prog. Mater. Sci.* **2013**, *58*, 1103−1172.
(33) Hansen, J. P.; McDonald, I. R. *Theory of Simple Liquids*, 3rd ed.; Elsevier/Academic Press, 2006.
(34) Miracle, D. B. A structural model for metallic glasses. *Nat. Mater.* **2004**, *3*, 697−702.
(35) Sheng, H. W.; Luo, W. K.; Alamgir, F. M.; Bai, J. M.; Ma, E. Atomic packing and short-to-medium-range order in metallic glasses. *Nature* **2006**, *439*, 419−425.
(36) Singh, S.; Ediger, M. D.; de Pablo, J. J. Ultrastable glasses from in silico vapour deposition. *Nat. Mater.* **2013**, *12*, 139−144.

https://dx.doi.org/10.1021/acs.jpclett.0c01789
J. Phys. Chem. Lett. 2020, 11, 6718−6723